Journal of Infrared, Millimeter, and Terahertz Waves (2021) 42:357–370
https://doi.org/10.1007/s10762-021-00785-8

INVITED REVIEW ARTICLE

Propagation Channel Measurements in the mm- and Sub-mm Wave Range for Different Indoor Communication Scenarios

M. A. Salhi · T. Kleine-Ostmann [1] · T. Schrader [1]

Received: 15 January 2021 / Accepted: 11 March 2021 / Published online: 24 March 2021

Abstract
Increasing data rates in wireless communications are accompanied with the need for new unoccupied and unregulated bandwidth in the electromagnetic spectrum. Higher carrier frequencies in the lower THz frequency range might offer the solution for future indoor wireless communication systems with data rates of 100 Gbit/s and beyond that cannot be located elsewhere. In this review, we discuss propagation channel measurements in an extremely broad frequency range from 50 to 325 GHz in selected indoor communication scenarios including kiosk downloading, office room communication, living rooms, and typical industrial environments.

Keywords Broadband indoor communications · Electromagnetic wave propagation · Millimeter waves · THz frequency range · Terahertz communications · Vector network analysis channel sounding

1 Introduction

Data rates in wireless communications are increasing exponentially, doubling approximately every 18 months [1, 2]. It can be foreseen that applications such as wireless backhaul and fronthaul links, kiosk downloading, wireless close proximity links, wireless data center links, or wireless chip-to-chip communication will make use of mm and sub-mm waves in order to enable data rates of 100 Gbit/s and beyond, reaching transmission capabilities of fiber-optical systems. The first standard for wireless communications operating in the frequency range of 252 to 325 GHz has been published by IEEE 802 in 2017 [3]. Under Agenda Item 1.15 of the last World Radio Conference (WRC) 2019 in Sharm El Sheikh, Egypt, regulatory activities were ongoing.

✉ T. Kleine-Ostmann
thomas.kleine-ostmann@ptb.de

[1] Department High Frequency and Electromagnetic Fields, Physikalisch-Technische Bundesanstalt (PTB), Bundesallee 100, 38116 Braunschweig, Germany

The physical challenges, such as path loss and atmospheric attenuation, and technological hurdles, such as excessive losses of waveguides and antennas, phase noise effects and lack of powerful sources, and low noise mixers and detectors, are much higher compared to lower frequencies. As a result of this, a THz communication system cannot be just a scaled version of a lower frequency system but requires a different architecture, e.g., using non-line of sight paths. High antenna gain is indispensable to mitigate the high path losses. Phased array beam forming seems to be the only feasible solution to establish reliable links in non-static scenarios where beam blocking is possible [4]. Appropriate approaches for beam acquisition and tracking will be essential. Channel characteristics and system design become heavily linked and can no longer be considered separately. Appropriate characterizations of system components including especially the propagation channel are crucial for the abovementioned challenges. Accurate and precise measurements of propagation, component, and signal characteristics will require the application of metrological methods including a rigorous uncertainty analysis [5] and establishing traceability to the international system of units (Système international d'unités (SI)) [6].

Channel sounding aims to characterize a dynamic channel about its relevant propagation paths [7]. At lower frequencies, where omni-directional transmitter and receiver schemes are predominating, this means measuring power delay profiles and extracting relevant parameters such as mean delay, delay spread and Doppler shift from the measured channel impulse responses. With increasing frequency, the propagation direction becomes relevant. E.g., sector antennas are used in mobile communication systems to increase coverage and efficiency. This adds the parameters direction-of-departure (DoD) and direction-of-arrival (DoA) to the classical time-of-flight (ToF) characterization in channel sounding. While dynamic high-bandwidth channel sounding is a well-established technique at frequencies of up to a few GHz [8, 9], only few studies exist in the mm wave or even the THz frequency range [10–14]. As it turns out that the different parameters (ToF, DoA, DoD, and Doppler shift) are mutually dependent, channel sounding becomes a problem of joint multidimensional parameter estimation [15–17]. It is subject of ongoing research to optimize resolution, precision, and accuracy and to establish traceability to the SI, which is a prerequisite for reliable quantitative extraction of channel parameters with known measurement uncertainty. The US national metrology institute (The National Institute of Standards and Technology (NIST)) has launched the 5G mm-wave channel model alliance and works on a white paper on verification techniques for channel sounders in the 5G standard [18]. The metrology of THz communications, including metrics for channel characterization and traceability of channel properties but also the metrology for signal measurements and many other metrological aspects are a main goal of ongoing research [19].

Channel sounding becomes much easier, when the channel properties are quasi-static. In case the channel does not change on a sub-second time scale, the propagation properties can be obtained from transmission measurements between antennas using vector network analysis (VNA). The band limited channel impulse response can be obtained from a Fourier transform of the measured transmission scattering parameter S_{21}. As VNA-based measurements are well established with traceability to the SI up to 170 GHz [6, 20, 21] and high signal-to-noise ratio, they can be used to verify or even calibrate channel sounders.

VNA-based propagation channel measurements in slowly time-variant indoor environments have been performed based on antennas and rotary stages that allow for angle-of-arrival characterization [22, 23]. Measurements have either been done in the baseband after up- and-down conversion with a versatile 300-GHz measurement system [24] or by using

frequency extension modules [22]. Investigated channels by different groups include typical indoor environments [22–26], outdoor environments [27], as well as wireless propagation in office devices [28]. The effect of diffraction on the propagation has been examined, and it has been shown that diffraction effects can be described with knife edge models and uniform geometrical theory of diffraction sufficiently well [29]. Diffraction effects as well as reflection properties measured for smooth [30] and rough [31, 32] surfaces in THz spectrometers have been incorporated in a ray-tracing tool that can be used to predict the coverage in indoor environments [33].

In this review, the results of a comprehensive measurement campaign including VNA-based propagation measurements in kiosk downloading, office room communication, living rooms, and typical industrial scenarios are presented. For the first time, the measurements cover the whole frequency range between 50 and 325 GHz, and the propagation is analyzed in detail in the frequency domain with regard to typical propagation paths and their losses. While initial measurements and discussions regarding the office environment [34, 35], the desktop download scenario [34–36], the industry environment [35] (no measurements), and the living room environment [23] were shown already, this paper contains additional measurement results covering the whole frequency range that have not been shown before for the living room and industry scenario and aims at a comprehensive discussion of the propagation conditions including human blockage.

The paper is structured as follows: after the introduction in Sect. 1, Sect. 2 describes the measurement setup. The following four chapters contain measurement results and discussion of the propagation phenomena in kiosk desktop downloading (Sect. 3), office room communication (Sect. 4), living rooms (Sect. 5), and typical industrial environments (Sect. 6). Then, observations and analysis are discussed (Sect. 7). The paper ends with a conclusion in Sect. 8.

2 Measurement Setup

All measurements are performed using a four-port vector network analyzer (R&S ZVA-50™) with five pairs of frequency extension modules (R&S ZVA-Z75…325™) operating in the waveguide bands WR-15, WR-10, WR-6, WR-5, and WR-3. The output flanges are equipped with standard gain horn antennas with 20 dB gain (Flann Series 240™). The dynamic range for measurements of the transmission $|S_{21}|$ exceeds 80 dB. The high-frequency (HF) cables were chosen to be long enough for the corresponding scenarios to enable multipoint propagation measurements. A vital advantage for VNA propagation measurements is the large available bandwidth, which varied here between 25 and 105 GHz according to the frequency extensions used.

An angular scanning resolution with 1° steps was chosen for the antenna rotation. The frequency scan was performed with 100-MHz steps using a fixed IF bandwidth of 10 kHz in all cases. With these settings, a measurement consisting of frequency scans for 360 different angular orientations of the rotated antenna took between 15 min for the WR-15 band and 50 min for the WR-3 band.

Before the measurements, full two-port calibration has always been performed for each set of frequency converters. Additionally, a source power calibration has been done to guarantee that the converters are in the optimum operating point.

The frequency extension modules are connected to the VNA and are fixed on supported holders mounted on top of rotating stages as shown in Fig. 1, whereas the motors are

controlled with a software written in LabVIEW™. The rotation stages are mobile and can be placed on any planar surface, constrained by the HF cable length, only, which was between 200 and 500 cm, depending on the propagation scenario.

The rotation stages are portable, and their lateral positions are adjustable via a lateral knob, additionally. The antenna apertures are surrounded by absorber material to minimize unwanted multiple signal reflections from the metal housings. For the measurements, an uncertainty of about 0.5 dB is estimated based on general observation of the hardware including antenna calibration and considering the stability of the VNA. Further factors such as misalignment would of course increase this estimated value.

3 Kiosk Desktop Download Scenario

This scenario initially introduced in [34–36] represents a desktop link between office devices communicating with each other, e.g., a laptop with an external hard disk. In a typical desktop download scenario, both transmitter Tx and receiver Rx are usually located on a common table and have a short line-of-sight propagation path in between each other in a constellation like that depicted in Fig. 1.

Figure 2a depicts the top view of the arrangements examined in this kiosk download scenario. Rx is placed 50 cm away from the Tx and then shifted to the left by 15 cm from the direct perpendicular line of sight (LOS). This placement allows scanning areas with strong and weak signals. The angular sweep was done from − 20° to + 20° with respect to the perpendicular line to Rx with 1° angular resolution resulting in 41 measurements in each frequency band. Figure 2 b illustrates the result presentation in frequency and angle in polar coordinates, where f is plotted on the radial axis and the angle is represented by the polar axis. This polar representation has the advantage of providing a visual impression of the propagation paths. The value of magnitude and unwrapped phase is presented according to the shown color bars. In Fig. 2 c, the measured magnitude (left) and phase (right) of the transmitted signal is shown for all five frequency bands covering 50 to 325 GHz. The figure reveals from the

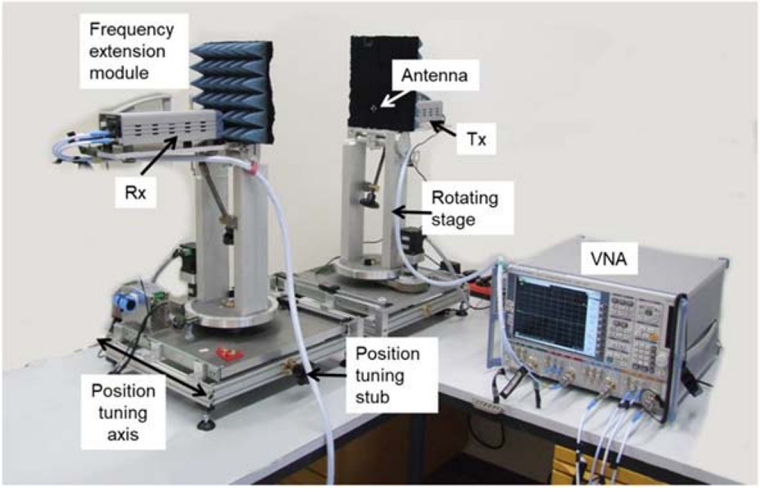

Fig. 1 Illustration of the measurement equipment (revised from [23, 36])

magnitude that with increasing frequency, the received power decreases, and the beam directivity increases. The phase is plotted in degrees with unwrapped angles above 180° given as multiples of 360°. One can notice that the phase increases by increasing the frequency. It can also be seen that the phase span changes from 300° in the 50–75-GHz (WR15) band and increases to reach about 600° in the 220–325-GHz band. Moreover, in the highest frequency band (WR3) close to − 20° scanning angle, the measured phase is in the noise region and therefore meaningless.

4 Office Scenario

One of the most relevant scenarios for future sub-millimeter wave indoor communications is a transmission link within an office room as introduced originally in [34, 35]. This implies that both Tx and Rx establish a directed path for transmission with high data rate over a short propagation distance. Figure 3a shows a schematic of the measurement room depicting the furniture and the measurement positions for both Tx and Rx. The strength of the received signal may vary depending on composition and position of the objects available in the room.

Signals from direct LOS and NLOS paths are contributing to the measured overall signal. Tx was scanned angularly up to 360° around the axis of the motor, while the reception antenna was kept at a fixed steering. The signal was measured at three different positions of the transmitter: P1, P2, and P3. The distances between Rx and these points are as follows $d_{\text{Rx-P1}} = d_{\text{Rx-P3}} = 236$ cm, and $d_{\text{Rx-P2}} = 200$ cm, whereas the lateral distances are $d_{\text{P1-P2}} = d_{\text{P2-P3}} = 125$ cm.

The measurement results are shown in Fig. 3b. The channel transfer function represented by the transmission parameter $|S_{21}|$ of the different frequency bands is depicted in the figures from

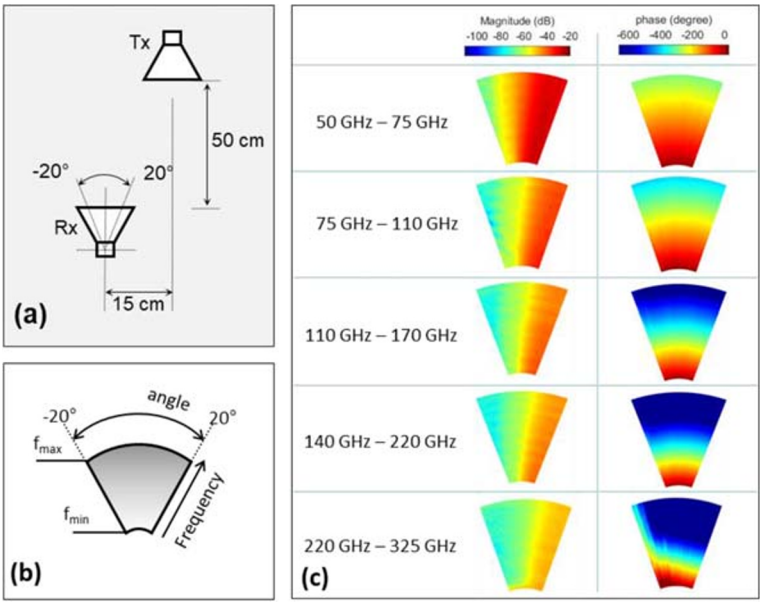

Fig. 2 **a** Schematic top view of the measurement in the desktop environment. Rx is rotated in the horizontal plane from − 20° to + 20°. **b** Illustration of frequency and angle dependent result representation. **c** The measured magnitude and phase for the given five frequency bands (revised from [34–36] and extended)

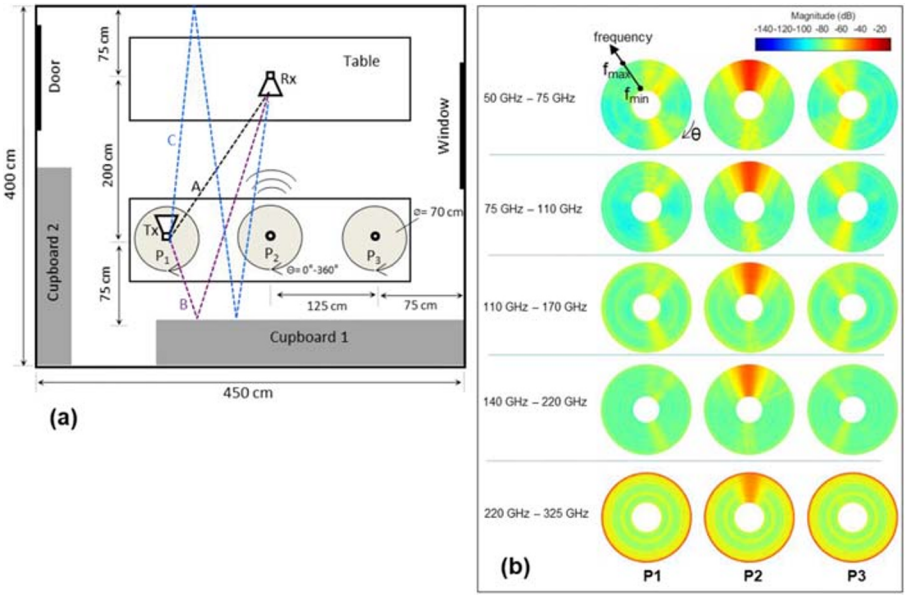

Fig. 3 **a** Schematic top view of the measurement office room. **b** $|S_{21}|$ measured at three positions for the given five frequency bands from 50 to 325 GHz. The data plot is illustrated in the first plot (top left). Revised from [34, 35]

(a) 50–75 GHz to (e) 220–325 GHz. For each frequency, $|S_{21}|$ is plotted as a circle, such that for the whole frequency range, a disk is formed in which the frequency increases with the radius of this disk and the angular coordinate represents the angle of rotation. In each measurement, Tx was rotated 360° with an angular resolution of 1°. At each distinct rotation angle, a frequency scan was done, and as a result, 360 measurements were obtained at each position for each frequency band. In the results, signals from LOS paths as well as from reflections can be identified. Although the transmission through direct LOS paths is the strongest in all frequency bands, reflections are significant as well. It is also noticed that the strength of reflections is frequency dependent even within the individual frequency bands and decreases in the higher frequency bands, mainly due to the increasing antenna directivity.

Due to the limited measurement dynamics and inadequacies in the system error correction of the VNA at higher frequencies, artifacts appearing as darker lines are observed in the frequency range 220–325 GHz.

5 Living Room Scenario

A transmission link within a home environment analogue to the known wireless local area network (WLAN) is an attractive application for high-speed communications. This requires a directed path for transmission between transmitter and receiver with high data rates but a relatively short propagation distance. To investigate this living room scenario, a room with suitable furniture was prepared as initially introduced in [23]. The room as shown in Fig. 4a contained tables, chairs, cabinets for books and dinnerware, and a flat screen TV.

Tx and Rx were both mounted on rotational units at 310-cm distance from each other. The height from the ground for both Tx and Rx was 190 cm and 72 cm, respectively, as illustrated in Fig. 4b. This difference in height has been established to simulate the conditions of a WLAN communication link. In the room most of the existing components, except the cupboards, were located below the antennas' level. The propagation was measured by scanning Rx by 360°, while Tx was placed at different fixed angles. Here, we only present the results for a Rx orientation of 45°.

Figure 4c shows the magnitude and phase of the propagating signal, respectively. The shown frequency range has been restricted to the WR-5 band, where representative results were obtained. The radius of the circle starts with 140 GHz at the inner radius and increases with frequency to reach 220 GHz at the outer circle. There, more than one path is observed. The darker red color in Fig. 4c indicates stronger signal levels. The dominant direct LOS path is marked as B1, whereas B2 refers to a strong NLOS path which is, most probably, facing a single reflection. The weak path marked as B3 is expected to be a result of multireflections in the room. Scattering at the measurement equipment or at the walls and the available furniture is the reason for such multipath propagation.

6 Industrial Scenario

This data communication scenario is especially interesting for its relevance in industrial applications such as in automating production and assembly lines, and in process control and monitoring. This scenario resembles an industry environment with an elongated passage including a guarded metallic stair, a wooden cupboard, and a switch cabinet, in addition to the

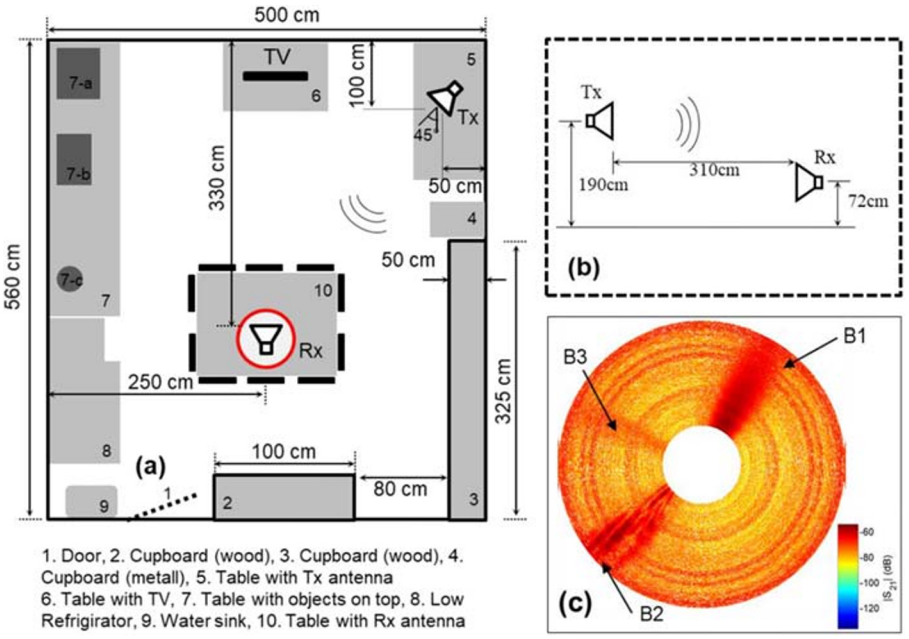

Fig. 4 **a** Schematic top view and **b** side view of the imitated living room including typical objects in such environments. **c** Measured magnitude of S_{21}. Revised from [23]

measurement equipment and its accessories. Moreover, the passage has three metallic doors, two of them are in the ground floor, and one is in the first floor at the top of the metallic stairs as detailed in Fig. 5a and initially shown in [35]. The passage is 800 cm high, 250 cm wide, and 800–850 cm long.

A remarkable feature of this scenario is the long propagation path compared to the previous scenarios with both Tx and Rx placed each at one side of the passage at 560-cm distance.

Among the most informative measurements is the one shown in Fig. 5b. The frequency range has been restricted to the WR-6 band, where representative results were obtained. It shows the measured $|S_{21}|$ when Rx is fixed at − 45° with the indicated orthogonal projection line. Here, the multiple paths are present with relatively high power due to the reflections on the metallic surfaces. It is also seen that more than one NLOS path is present, which occurs due to the multiple reflections or due to the partial reflection of the beam.

To have a closer look at this measurement, a single frequency has been selected indicated by the black circle marked in Fig. 5b. At 149 GHz, the azimuth angle range of 360° shows clear peaks at Tx angles of − 44°, 49°, and 125° (Fig. 5c). Not all of these peaks are present at other frequencies, since the reflection is frequency selective.

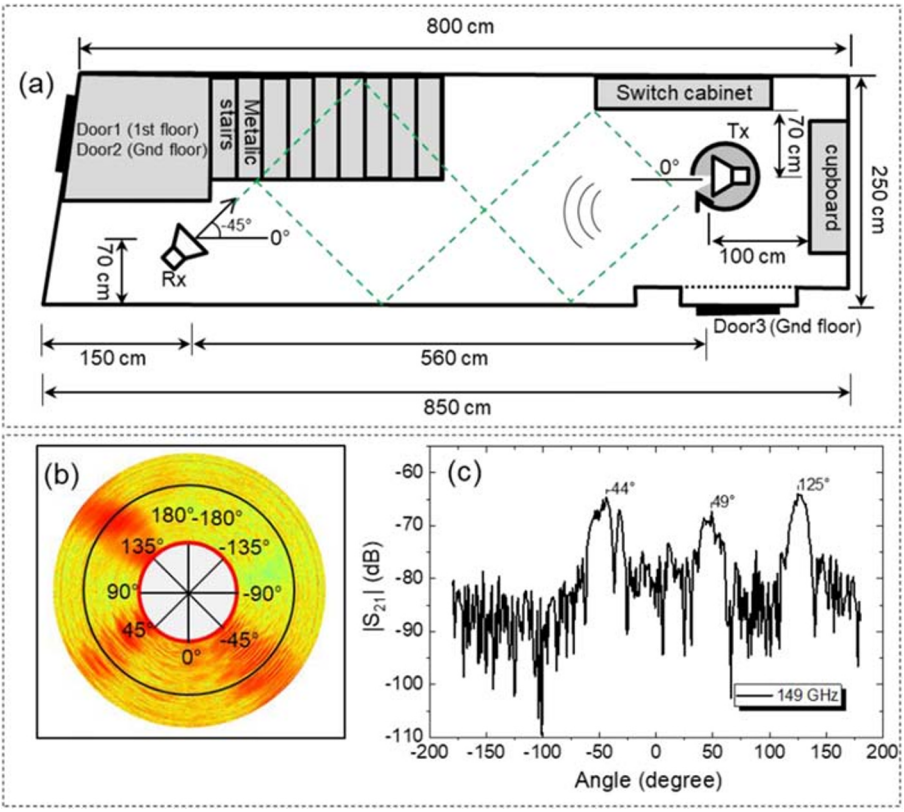

Fig. 5 **a** Schematic of the measurement location for industrial scenario. **b** Polar representation of $|S_{21}|$ for 110–170 GHz. **c** The Cartesian representation of $|S_{21}|$ at 149 GHz. Revised from [35] and extended

7 Observation and Analysis

In the following subsections we present an investigation on the behavior of the propagating radiation by comparing the different scenarios, and give analysis with respect to reflection and interference, path loss, and finally influence of antenna directivity.

7.1 Comparison Between the Scenarios

Generally, submillimeter waves are suitable for indoor and short-range communications. The mainly targeted indoor scenarios here are typical examples for such environments. These scenarios do vary slightly by their impact on the path length and scattering and reflections of the beams.

Figure 6 shows a comparison between $|S_{21}|$ when one antenna is at a fixed transmission angle in the office, living room, and industrial environment scenario. The constellations for the measurements are depicted in Fig. 6a, where both antennas are not facing each other, but are rather displaced. Yet, a direct LOS path is still existing. This has the advantage of resembling a real communication link with multipath propagation. The measured propagation signals are shown in polar plot in Fig. 6b below each scenario. Since propagation is frequency selective, we compare $|S_{21}|$ averaged over the whole frequency band as seen in Fig. 6c. There, the channel response for the scenarios is given in a stacked graph. In the office scenario, we see two peaks almost similar in magnitude and another smaller peak. In the other scenarios (living room and industry), we see one main path and more than one smaller paths. The signal-to-noise ratio in all scenarios is about 10 dB and the maximum signal level is − 70 dB. We conclude that all three scenarios show quite similar propagation behavior with several paths in each, despite differing furniture with deviating reflection properties.

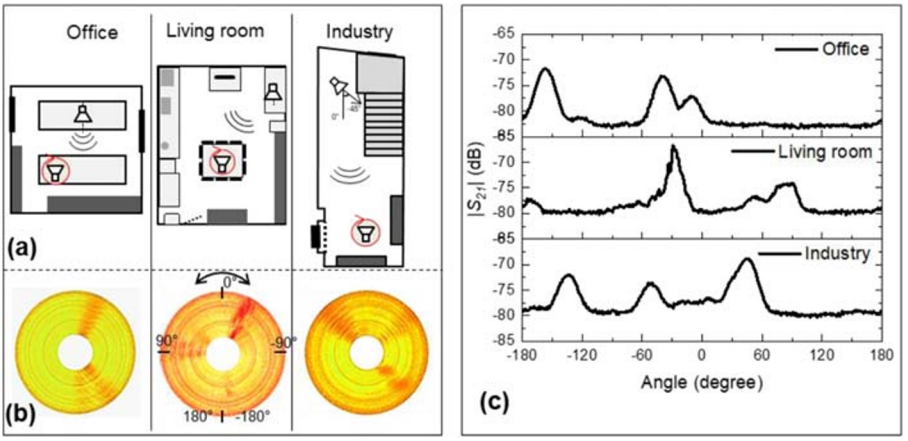

Fig. 6 A comparison between three scenarios when Tx and Rx are laterally shifted. **a** The constellation for the measurement scenarios and **b** the corresponding measured $|S_{21}|$. **c** The average value of the measured magnitude at the receiver for the whole frequency range (140–220 GHz)

7.2 Interference of Propagating Beams

Operating Tx and Rx on top of a reflecting plane will lead to a remarkable influence according to the electromagnetic propagation theory. To investigate this effect, a 50 cm × 60 cm metallic plate was placed 5 cm below the antenna centers. A metallic plate is an almost perfect reflector in the THz frequency range and represents the extreme assumption for the reflectivity of a table. The transfer function $|S_{21}|$ was measured for the Tx positions P1, P2, and P3 which are 15 cm away from each other over short distance to Rx ($d_{\text{Rx-P2}} = 50$ cm and $d_{\text{Rx-P1}} = d_{\text{Rx-P3}} = 52$ cm) with scanning angles from − 20° to 20° of the Tx antenna as illustrated in Fig. 7a and b.

Figure 7c depicts $|S_{21}|$ as measured in free space (60 cm above the wooden table) without (top) and with (bottom) the metallic plate for the frequency band 220–325 GHz. As expected, $|S_{21}|$ decreases with increasing the angle of deviation of Tx from the line-of-sight. The measurement agrees well with Friis' transmission formula, considering the angle dependent antenna gain.

Then, we took a cross section at the dashed line shown at P2 to analyze the behavior of $|S_{21}|$ in more detail in Fig. 7d. The red curve shows $|S_{21}|$ after installing the metallic plate in the horizontal plane 5 cm below the antennas. The difference between the minimum and maximum value of $|S_{21}|$ reaches 10 dB above 300 GHz. The metallic plate leads to reflections and hence multipath propagation and interference of the directly propagating waves with those reflected from the plate. These interference patterns get more pronounced as the frequency increases.

7.3 Reflections Due to Human Obstacles

As at mm-waves the transmission is highly directive and the human body acts as absorber. The propagation of electromagnetic waves is highly affected by the presence of people. The effect of human blockage including dynamic link behavior has been examined in detail at 60 GHz [37]. Here, we briefly discuss the effect by comparing two measurements with and without a person in the living room scenario introduced earlier. Here the person stood stationary blocking a small part of the LOS beam between both Tx and Rx as demonstrated in Fig. 8a. The measured $|S_{21}|$ for a full angular scan in the frequency range 140–220 GHz is depicted in Fig. 8b with a close-up for the LOS beam. There, artifacts are observed. However, more clearly are they seen when analyzing the amplitude difference in Fig. 8c and the phase difference in Fig. 8d. Here, we see about ± 5 dB difference in amplitude and ± 3° difference in phase mainly at a Rx angle between − 20° and 45° and slight artifacts at 130°–140°.

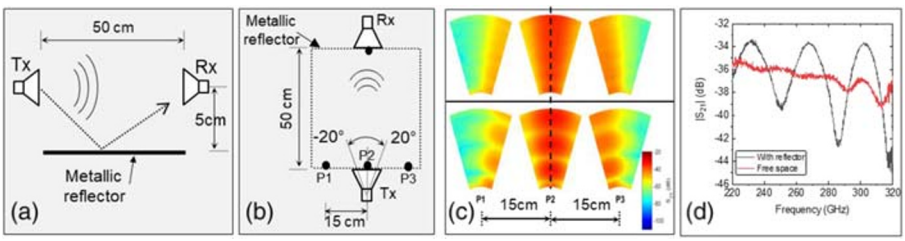

Fig. 7 **a** Top view and **b** side view schematic of the measurement setup for investigating the reflection effect. **c** 2D channel response ($|S_{21}|$) for the frequencies 220–325 GHz without (top) and with a metallic plate. The points P1, P2, and P3 indicate the positions of the Tx. **d** $|S_{21}|$ at P2 as indicated in the dashed line in **c**

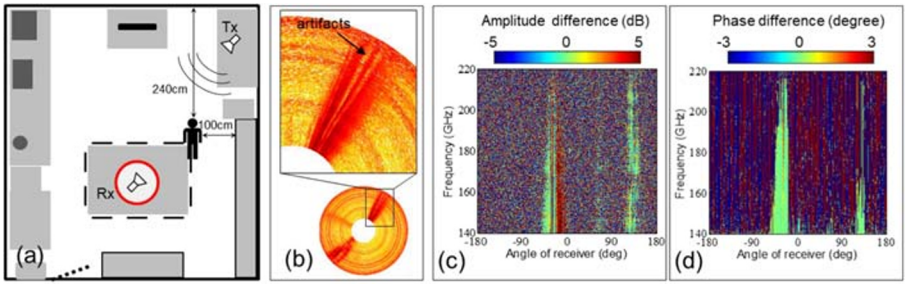

Fig. 8 **a** Schematic of the measurement room in the presence of a person. **b** The measured $|S_{21}|$ with a closeup in the LOS beam region. **c** The amplitude difference and (d) phase difference between the transmission with and without a person in the room

For a non-stationary person, Doppler frequency shift should be considered. However, it is one of the limitations of VNA channel sounding that only static measurements can be analyzed.

7.4 Path Loss

Atmospheric absorption and scattering are basic decay effects of propagating THz radiation which occur mainly due to the existing water molecules in air. The attenuation increases with frequency [1]; however, there are several windows which give the potential for this radiation to be used in short- and medium-range communication systems.

Figure 9 shows the channel transfer function of the center frequencies for the five frequency bands used here, namely at 62.5 GHz, 92.5 GHz, 140 GHz, 180 GHz, and 272.5 GHz. In Fig. 9a, we see $|S_{21}|$of the received signal at propagation distances between 50 and 80 cm.

Considering that the propagating waves pass a distance from $d_1 = 50$ cm to $d_2 = 80$ cm, then the path loss within these 30 cm can be obtained from Fig. 9a by taking the difference of S_{21} at these distances for each frequency according to the equation:

$$Path\ loss = S^{dB}_{21,d=50cm} - S^{dB}_{21,d=80cm}$$

These data are extracted and presented in the in the solid line in Fig. 9b. The dashed line is the theoretical path loss calculated according to Friis formula [38]:

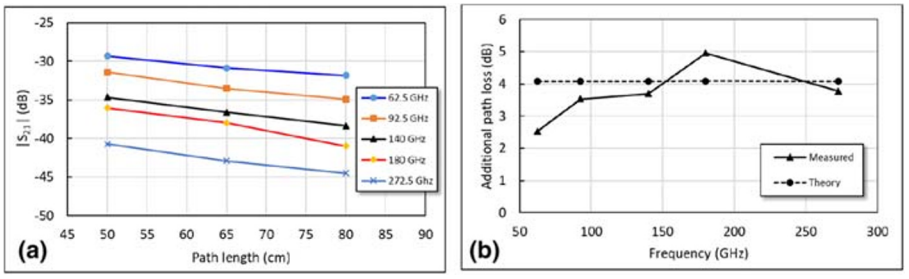

Fig. 9 **a** Free space transmission $|S_{21}|$ between Tx and Rx at different receiver positions and frequencies. **b** The attenuation when increasing the distance between Tx and Rx from 50 to 80 cm

$$\frac{P_{Rx}}{P_{Tx}} = \left(\frac{c}{4\pi d_i f}\right)^2 \cdot G_{Tx} \cdot G_{Rx}$$

and in dB the equation is as follows:

$$P_{Rx}^{dB} = P_{Tx}^{dB} + G_{Tx}^{dB} + G_{Rx}^{dB} + 20\log_{10}\left(\frac{c}{4\pi d_i f}\right)$$

Knowing that the gain of both horn antennas $G_{\mathrm{Tx}} = G_{\mathrm{Rx}} = 20$ dB, and distance $d_1 = 50$ cm, $d_2 = 80$ cm, c is the speed of light, f is the frequency, P_{Rx} is the received power, and P_{Tx} is the transmitted power, the path loss within these 30 cm is found as follows:

$$Pathloss_{\Delta d}^{dB} = P_{Rx,d=50cm}^{dB} - P_{Rx,d=80cm}^{dB} = 20\log_{10}\left(\frac{\mathrm{c}}{4\pi f d_{50cm}}\right) - 20\log_{10}\left(\frac{c}{4\pi f d_{80cm}}\right) \approx 4.08\ dB$$

The path loss here is found to be 4.08 dB which in line with the measured ones. However, deviations up to 1.5 dB occur in this transmission configuration.

8 Conclusion

In this review, we presented broadband channel propagation measurements in a typical kiosk, office, living room, and in an industrial environment scenario. The measurements were based on a commercial vector network analyzer and frequency extension modules which generate signals at frequencies from 50 up to 325 GHz radiated via standard gain horn antennas. Rotational stepper motors were employed to scan Tx and/or Rx angularly up to 360°.

The magnitude and phase results showed that the LOS waves are dominating in all scenarios, whereas the reflected signals are significantly appearing in the propagation and cannot be neglected. We discussed the propagation channel considering the path loss and the existence of metallic reflectors and persons.

Acknowledgments The authors would like to thank Sebastian Priebe, Martin Jacob, Sebastian Rey, Alexander Fricke, and Prof. Thomas Kürner, all with the Institute for Communications Technology at Technical University Braunschweig, for providing the rotation stages for automated measurements as part of the very fruitful cooperation on THz communications research. Furthermore, the authors acknowledge discussions on new signal measurement techniques with Prof. Thomas Schneider from the Institute for Radio Frequency Engineering at Technical University Braunschweig and on channel sounding techniques with Prof. Reiner Thomä from Technical University Ilmenau within the DFG research group FOR 2863 – Metrology for THz Communications (Meteracom).

Author Contribution All authors contributed to the study conception and design. Material preparation, data collection, and analysis were performed by Mohammed Salhi. The first draft of the manuscript was written by Mohammed Salhi and Thomas Kleine-Ostmann, and all authors commented on previous versions of the manuscript. All authors read and approved the final manuscript.

Funding Open Access funding enabled and organized by Projekt DEAL. This work was funded within the European Metrology Research Programme (EMRP) in the Joint Research Project IND16 Ultrafast – Metrology for ultrafast electronics and high-speed communications. The EMRP is jointly funded by the EMRP participating countries within EURAMET and the European Union.

Declarations

Availability of data and material
Upon request.

Conflict of Interest The authors declare that they have no conflict of interest.

References

1. T. Kleine-Ostmann and T. Nagatsuma, A Review on Terahertz Communications Research, Journal of Infrared, Millimeter, and Terahertz Waves, vol. 32, pp. 143-171, 2011.
2. Kürner, T., Priebe, S. „Towards THz Communicatons – Status in Research, Standardisation and Regulation“, Journal of Infrared, Millimeter, and Terahertz Waves, vol. 35, no. 1, pp. 53-62, 2014.
3. IEEE 802.15.3d-2017 – IEEE Standard for High Data Rate Wireless Multi-Media Networks Amendment 2: 100 Gb/s Wireless Switched Point-to-Point Physical Layer, https://doi.org/10.1109/IEEESTD.2017.8066476.
4. R. Piesiewicz, T. Kleine-Ostmann, N. Krumbholz, D. Mittleman, M. Koch, J. Schöbel and T. Kürner, Short-range ultra broadband terahertz communications: concept and perspectives, IEEE Ant. Prop. Mag., vol. 49, pp. 24-39, 2007.
5. Evaluation of measurement data – Guide to the expression of uncertainty in measurement, JCGM 100:2008, GUM 1995 with minor corrections.
6. T. Kleine-Ostmann, T. Schrader, M. Bieler, U. Siegner, C. Monte, B. Gutschwager, J. Hollandt, A. Steiger, L. Werner, R. Müller, G. Ulm, I. Pupeza and M. Koch, THz Metrology, Frequenz, vol. 62, pp. 137-148, 2008.
7. A. F. Molisch, Wireless Communications, Wiley & Sons, 2007.
8. J. Fuhl, J. P. Rossi, and E. Bonek, “High-resolution 3-D direction-of arrival determination for urban mobile radio,” IEEE Trans. Antennas Propagat., vol. 45, pp. 672–671, 1997.
9. Y. L. C. de Jong and M. H. A. J. Herben, “High-resolution angle-of arrival measurement of the mobile radio channel,” IEEE Trans. Antennas Propagat., vol. 47, pp. 1677–1687, 1999.
10. S. Kim, W. T. Khan, A. Zajić, and J. Papapolymerou, “D-band channel measurements and characterization for indoor applications,” IEEE Transactions on Antennas and Propagation, vol. 63, no. 7, pp. 3198-3207, 2015.
11. J.T. Quimby, D. Williams, K.A. Remley, P.B. Papazian, D. Ribeiro, and J. Senic, “Metrology-Grade Channel Sounder Verification at mmWave Frequencies,” 32nd URSI GASS, Montreal, 19-26 August 2017.
12. R. Sun, P. Papazian, J. Senic, Y. Lo, J. Choi, K.A. Remley, and C. Gentile, “Design and Calibration of a Double-directional 60 GHz Channel Sounder for Multipath Component Tracking,” European Conference on Antennas and Propagation, EuCAP 2017, 19-24 March, Paris, France.
13. S. Rey, J. M. Eckhardt, B. Peng, K. Guan and T. Kürner, "Channel sounding techniques for applications in THz communications: A first correlation based channel sounder for ultra-wideband dynamic channel measurements at 300 GHz," 2017 9th International Congress on Ultra Modern Telecommunications and Control Systems and Workshops (ICUMT), Munich, 2017, pp. 449-453.
14. R.S. Thomä, D. Hampicke, A. Richter, G. Sommerkorn and U. Trautwein, “MIMO Vector Channel Sounder Measurement for Smart Antenna System Evaluation,” European Trans. on Telecommunic. ETT, vol. 12, no. 5, Sept./Oct. 2001, pp. 427-438
15. R. Wang, O. Renaudin, C. U. Bas, S. Sangodoyin, and A.F. Molisch, “High-Resolution Parameter Estimation for Time-Varying Double Directional V2V Channel,” IEEE Trans. on Wireless Communications, vol. 16, no. 11, pp. 7264-7275, 2017.

16. M. Haardt, R. Thomä and A. Richter, “Multidimensional High-Resolution Parameter Estimation with Applications to Channel Sounding,” in Yingbo Hua (Ed.), High-Resolution and Robust Signal Processing, Marcel Dekker, 2003, pp. 253-337
17. R. Müller, S. Häfner, D. Dupleich, R.S. Thomä, G. Steinböck, J. Luo, E. Schulz, X. Lu, G. Wang, "Simultaneous Multi-Band Channel Sounding at mm-Wave Frequencies," EUCAP 2016, 10-15 April 2016, Davos, Switzerland
18. K. Remley, Ed., “Verification Techniques for mmWave Channel Sounders 5G,” White paper of mmWave Channel Model Alliance.
19. D. Humphreys, M. Berekovic, I. Kallfass, C. Scheytt, T. Kuerner, A. Jukan, T. Schneider, T. Kleine-Ostmann, M. Koch, R. Thomae, An overview of the Meteracom Project. In: Proc. 43-nd Meeting of the Wireless World Research Forum (WWRF), London, UK, Okt. 2019.
20. T. Schrader et al., Verification of scattering parameter measurements in waveguides up to 325 GHz including highly-reflective devices, Adv. Radio Sci. 9, 9–17 (2011).
21. D. F. Williams, 500 GHz –750 GHz Rectangular-Waveguide Vector-Network-Analyzer Calibrations, IEEE Trans. THz Sci. Techn. 1, 364-377 (2011).
22. S. Priebe, C. Jastrow, M. Jacob, T. Kleine-Ostmann, T. Schrader and T. Kürner, Channel and Propagation Measurements at 300 GHz, IEEE Trans. on Antennas & Propagation, vol. 59, pp. 1688-1698, 2011.
23. M. Salhi, T. Kleine-Ostmann and T. Schrader, Antenna Characterization and Channel Measurements in the mm Wave and Sub-mm Wave Region, Microwave Journal 58, 124-134 (2015).
24. C. Jastrow, K. Münter, R. Piesiewicz, T. Kürner, M. Koch and T. Kleine-Ostmann, 300 GHz Transmission System, Electron. Lett. 44, 213-214 (2008).
25. S. Kim and A. G. Zajić, Statistical Characterization of 300-GHz Propagation on a Desktop, IEEE Transactions on Vehicular Technology 64, 3330 – 3338 (2015).
26. C.-L. Cheng, S. Sangodoyin and A. Zajić, THz Cluster-Based Modeling and Propagation Characterization in a Data Center Environment, IEEE Access 8, 56544-56558 (2020).
27. N. A. Abbasi, A. Hariharan, A. M. Nair, A. S. Almaiman, F. B. Rottenberg, A. E. Willner and A. F. Molisch, Double Directional Channel Measurements for THzCommunications in an Urban Environment, arXiv:1910.01381v1 (2019).
28. T. Kürner, A. Fricke, S. Rey, P. Le Bars, A. Mounir, and T. Kleine-Ostmann, Measurements and Modeling of Basic Propagation Characteristics for Intra-Device Communications at 60 GHz and 300 GHz, J Infrared Milli Terahz Waves 36, 144-158 (2015).
29. M. Jacob, S. Priebe, R. Dickhoff, T. Kleine-Ostmann, T. Schrader and T. Kürner, Diffraction in mm and sub-mm Wave Indoor Propagation Channels, IEEE Trans. on Microwave Theory and Techniques, vol. 60, pp. 833-844, 2012.
30. R. Piesiewicz, T. Kleine-Ostmann, N. Krumbholz, D.Mittleman, M. Koch, and T. Kürner, THz characterisation of building materials, El. Lett. 41, 1002-1004 (2005).
31. R. Piesiewicz, C. Jansen, D. Mittleman, T. Kleine-Ostmann, M. Koch and T. Kürner, Scattering analysis for the modeling of THz communication systems, IEEE Trans. on Antennas & Propagation, vol. 55, pp. 3002-3009, 2007.
32. C. Jansen, S. Priebe, C. Möller, M. Jacob, H. Dierke, M. Koch, T. Kürner: Diffuse scattering from rough surfaces in THz communication channels, IEEE Trans. Terahertz Sci. and Technol. 2, 462-472, 2011.
33. S. Priebe, M. Kannicht, M. Jacob, and T. Kürner: Ultra broadband indoor channel measurements and calibrated ray tracing propagation modeling at THz frequencies, J of Communications and Networks 15, 547-558, 2013.
34. M. Salhi, T. Kleine-Ostmann, T. Schrader, M. Kannicht, S. Priebe and T. Kürner, "Broadband channel measurements in a typical office environment at frequencies between 50 GHz and 325 GHz," 2013 European Microwave Conference, Nuremberg, 2013, pp. 175-178.
35. T. Kleine-Ostmann, M. Salhi, M. Kannicht, S. Priebe, T. Kürner and T. Schrader, "Broadband channel measurements between 50 GHz and 325 GHz: Comparison of different propagation scenarios," 2013 38th International Conference on Infrared, Millimeter, and Terahertz Waves (IRMMW-THz), Mainz, 2013, pp. 1-2.
36. M. Salhi, T. Kleine-Ostmann, M. Kannicht, S. Priebe, T. Kürner and T. Schrader, "Broadband channel propagation measurements on millimeter and sub-millimeter waves in a desktop download scenario," 2013 Asia-Pacific Microwave Conference Proceedings (APMC), Seoul, 2013, pp. 1109-1111.
37. M. Jacob, S. Priebe, A. Maltsev, A. Lomayev, V. Erceg, and T. Kürner. “A Ray Tracing Based Stochastic Human Blockage Model for the IEEE 802.11ad 60 GHz Channel Model”, 5th European Conference on Ant. and Prop. (EuCAP), Rome, Italy, pp. 1–5, 2011.
38. C. Balanis, Antenna theory. 1st ed. Hoboken, NJ: Wiley Interscience, 2005.